Open access • Journal Article • DOI:10.1021/ACS.INORGCHEM.6B03057

Synthesis of MAX Phases in the Zr-Ti-Al-C System — Source link

Bensu Tunca, Thomas Lapauw, Olesia M. Karakulina, Maria Batuk ...+5 more authors

Institutions: Katholieke Universiteit Leuven, University of Antwerp, University of Poitiers

Published on: 03 Mar 2017 - Inorganic Chemistry (American Chemical Society)

Topics: MAX phases and Solid solution

Synthesis of MAX phases in the Zr-Ti-Al-C system

Synthesis of MAX phases in the Zr-Ti-Al-C system

Bensu Tunca,[a,b*] Thomas Lapauw,[a,b] Olesia M. Karakulina,[c] Maria Batuk,[c] Thierry Cabioc'h,[d] Joke Hadermann,[c] Rémi Delville,[a] Konstantina Lambrinou,[a] and Jozef Vleugels[b]

[a] *SCK•CEN, Boeretang 200, B2400 Mol, Belgium*

[b] *KU Leuven, Department of Materials Engineering, Kasteelpark Arenberg 44, B-3001 Leuven, Belgium*

[c] *University of Antwerp, Department of Physics, Electron Microscopy for Materials Research (EMAT), Groenenborgerlaan 171, B-2020 Antwerp, Belgium*

[d] *Institut Pprime, UPR 3346, CNRS - Université de Poitiers - ENSMA, SP2MI, Téléport 2-BP 30179, 86962 Futuroscope Chasseneuil Cedex, France*

** Corresponding author. Address: SCK•CEN, Boeretang 200, B-2400 Mol, Belgium*

E-mail address: btunca@sckcen.be (B.Tunca)

ABSTRACT

This study reports on the synthesis and characterization of MAX phases in the $(Zr,Ti)_{n+1}AlC_n$ system. The MAX phases were synthesized by reactive hot pressing and pressureless sintering in the 1350-1700°C temperature range. The produced ceramics contained large fractions of 211 and 312 (n=1 and 2) MAX phases, while strong evidence of a 413 (n=3) stacking was found. Moreover, (Zr,Ti)C, $ZrAl_2$, $ZrAl_3$, and Zr_2Al_3 were present as secondary phases. In general, the lattice parameters of the hexagonal 211 and 312 phases followed Vegard's law over the complete Zr-Ti solid solution range, but the 312 phase showed a non-negligible deviation from Vegard's law around the $(Zr_{0.33},Ti_{0.67})_3Al_{1.2}C_{1.6}$ stoichiometry. High-resolution scanning transmission electron microscopy combined with X-ray diffraction demonstrated ordering of the Zr and Ti atoms in the 312 phase, whereby Zr atoms occupied preferentially the central position in the close-packed M_6X octahedral layers. The same ordering was also observed in 413 stackings present within the 312 phase. The decomposition of the secondary (Zr,Ti)C phase was attributed to the miscibility gap in the ZrC-TiC system.

Keywords

MAX phase ceramics; X-ray diffraction; Reactive hot pressing; Hydrides; Solid solution

MAX phases; Ordered MAX phases

1. INTRODUCTION

A class of fascinating ternary carbides and nitrides, later labelled MAX phases, was discovered in powder form in the 1960s[1] and gained renewed interest in the mid-1990s when manufacturing in the bulk form allowed the determination of their intrinsic properties.[1,2] MAX phases combine properties characteristic of metals, such as good thermal/electrical conductivity, thermal shock resistance, appreciable machinability, damage tolerance and relative softness, with properties characteristic of ceramics, such as good high-temperature mechanical properties and satisfactory resistance to oxidation and corrosion.[3] The stoichiometry of MAX phases is described by the $M_{n+1}AX_n$ general formula, where M is an early transition element, A is an A-group element, X is C or N and n is 1, 2 or 3.[4] MAX phases are layered hexagonal solids, with space group $P6_3/mmc$ (no. 194), their structure

consisting of near close-packed layers of M_6X octahedra interleaved with layers of A-group elements. The M_6X octahedra resemble the octahedra found in the cubic rock-salt structure of the corresponding binary MX carbides, and the number of M_6X layers actually determines whether the overall structure is 211, 312, or 413.

MAX phases in the Ti-Al-C system have already been extensively studied and are known for their outstanding oxidation resistance that results from the formation of a protective Al_2O_3 oxide scale.[5] Moreover, Zr-Al-C-based MAX phases, such as Zr_3AlC_2 and Zr_2AlC, have only been recently synthesized[6,7] and their properties are yet to be determined. The potential importance of Zr-Al-C MAX phases for the nuclear industry is associated with the low neutron cross-section of zirconium (Zr), which makes them promising candidate materials for fuel cladding applications. Especially in the post-Fukushima era, the development of accident-tolerant fuel (ATF) cladding materials that can outperform the zircaloy clads used in the current fleet of light water reactors is an important priority for the nuclear industry. These materials must combine superior resistance to aqueous corrosion and high-temperature steam oxidation with adequate radiation tolerance. Prior studies on the oxidation behaviour of Zr-Al-C compounds, such as $Zr_2[Al(Si)]_4C_5$ and $Zr_3[Al(Si)]_4C_6$, showed the formation of non-protective ZrO_2 oxide scales.[8] Similar studies on Ti-doped $Zr_2(AlSi)_4C_5$ ceramics revealed an improvement in oxidation resistance attributed to the addition of titanium (Ti).[9] Also, the addition of Zr to $Ti_3(Si_{0.95},Al_{0.05})C_2$ to form $(Ti_{1-x},Zr_x)_3(Si_{0.95},Al_{0.05})C_2$ up to x=0.07 resulted in an improvement of the high-temperature stiffness of the starting material.[10]

Several prior studies on MAX phases have demonstrated property improvement for the ternary compounds by the partial substitution of the elements on the M, A or X sites. Such substitution leads to the formation of solid solutions, some of them ordered, i.e., solid solutions where the added elements occupy a preferred atomic position.[11] Recent attempts to synthesize 211 MAX phases in the Zr-Ti-Al-C system were reported as unsuccessful[12] and no $(Zr_{1-x},Ti_x)_2AlC$ MAX phases have so far been experimentally reported. On the other hand, $(Zr_{1-x},Ti_x)_3AlC_2$ MAX phases were recently claimed to have been successfully synthesized, but the results of that study have not yet been published.[13] Solid solutions reported to contain Ti, Zr, Al and C include: $(Ti,M)_2AlC$ with M = V, Nb, Ta, Cr,[14–17] $(Nb,Zr)_2AlC$,[15,18] $(Ti,V)_3AlC_2$,[18] $(Ti,Nb)_4AlC_3$,[19] and $(Nb,Zr)_4AlC_3$.[20,21]

In this study, Ti was added to the Zr-Al-C system in an attempt to synthesize $(Zr_{1-x},Ti_x)_3AlC_2$ (ZT312) and $(Zr_{1-x},Ti_x)_2AlC$ (ZT211) MAX phase solid solutions. Different Ti contents were added in order to cover the whole Zr-Ti solid solubility range.

2. EXPERIMENTAL SECTION

2.1. Synthesis. ZrH_2 (<6 μm, >99% purity, Chemetall, Germany), TiH_2 (<8 μm; >99% purity; Chemetall, Germany), Al (<5 μm, >99% purity, AEE, United States) and C (<5 μm, >99% purity, Asbury Graphite Mills, United States) powders were used as starting materials for MAX phase synthesis. The Zr:Ti:Al:C ratio in the starting powder was [3(1-x)]:[3x]:[1.2]:[1.6] with x = 0, 0.1, 0.2, 0.5, 0.67, 0.7, 0.8, 0.9 and 1, so as to investigate a wide range of the Ti and Zr solid solubility on the M site of the produced MAX phases.

The initial stoichiometries were selected to target the 312 stoichiometry, using a slightly higher Al content to compensate for possible Al losses due to melting during processing, and a lower C content to compensate for C interdiffusion from the graphite die/punch setup of the hot press. The selection of the 312 stoichiometry was based on previous work on Zr-Al-C MAX phases[6,7] that showed an off-stoichiometric MAX phase formation, i.e., the synthesis of 211 and 312 MAX phases started from 312 and 413 initial starting powder mixtures, respectively. Powders were dry mixed for 48 hours in air, on a Turbula type multidirectional mixer. The powder mixtures were cold pressed at 30 MPa in a 30-mm inner-diameter graphite die setup. The powder compacts were hot pressed in vacuum (~10 Pa), using graphite punches in the same setup (W100/150-2200-50 LAX, FCT Systeme, Frankenblick, Germany). The heating rate was 25°C/min and the dwell time at the targeted 1350-1700°C range was 30 min, during which period the initial load of 7 MPa increased to 30 MPa. Pressureless sintering involved cold pressing powder compacts at 30 MPa that were subjected to the same thermal excursions as their hot pressed equivalents.

2.2. Characterization. Samples were produced for scanning electron microscopy (SEM) and transmission electron microscopy (TEM) examination and the remaining ceramics were ring-milled to obtain powders for X-ray diffraction (XRD). Backscattered electron (BSE) detector images of bulk samples were obtained on a FEI Nova NanoSEM, while high-resolution scanning transmission electron microscopy (HRSTEM) combined with energy dispersive X-ray spectroscopy (EDS) were employed to analyse thin foils on a FEI Titan^3 aberration-corrected transmission electron microscope (200 kV), using a high-angle annular dark-field (HAADF) detector. Thin-foil preparation for TEM analysis involved mechanical thinning with diamond lapping films and polishing down to 100 μm before final preparation to electron transparency with a JEOL Cryo Ion Slicer at 6 kV. The phase assembly in the produced MAX phase ceramics was determined by XRD (Seifert 3003), using Cu K_α radiation operated at 40

kV and 40 mA, and the XRD patterns were obtained from powder samples using a Bragg-Brentano geometry in the 5 to 75° 2θ range with a step size of 0.02° and a time of 2 s per step. Ordering in the produced MAX phases was studied by means of a Bruker D2 advanced diffractometer with Cu K_α radiation, operated at 30 kV and 30 mA in the Bragg-Brentano geometry, with a divergence slit of 0.6°, a 2θ step size of 0.02° and a time of 0.1 s, due to the higher peak to background ratio. Lattice parameters and weight fractions of phases were determined by Rietveld refinement of the powder XRD patterns, using the Materials Analysis Using Diffraction (MAUD) software.[22] XRD pattern simulations were performed using the PowderCell software.[23]

3. RESULTS AND DISCUSSION

3.1. Pressure-assisted MAX phase synthesis. The use of powder mixtures with an initial $(Zr_{1-x},Ti_x)_3Al_{1.2}C_{1.6}$ stoichiometry and x varying between 0 and 1 resulted in the synthesis of both the 211 (ZT211) and 312 (ZT312) MAX phases. Furthermore, local 413 stackings were observed inside 312 grains examined by HAADF STEM, as will be demonstrated later in the text.

Figure 1 shows the evolution of the different types of MAX phases (ZT211 and ZT312) as a function of the hot-pressing temperature and atomic fraction, x, of Ti in the $(Zr_{1-x},Ti_x)_3Al_{1.2}C_{1.6}$ starting powder. The phase assemblies of all hot pressed ceramics are presented as pie charts, where different colours are used to indicate the different phases identified by XRD analysis. All ceramics contained Zr- and/or Ti-rich ternary (Zr,Ti)C carbides, whereas only the Zr- and Ti-based end members contained binary ZrC and TiC, respectively. The secondary carbides are addressed in a dedicated section below. $ZrAl_2$, $ZrAl_3$ or Zr_2Al_3 intermetallics were also observed in some of the ceramics hot pressed below 1550°C.

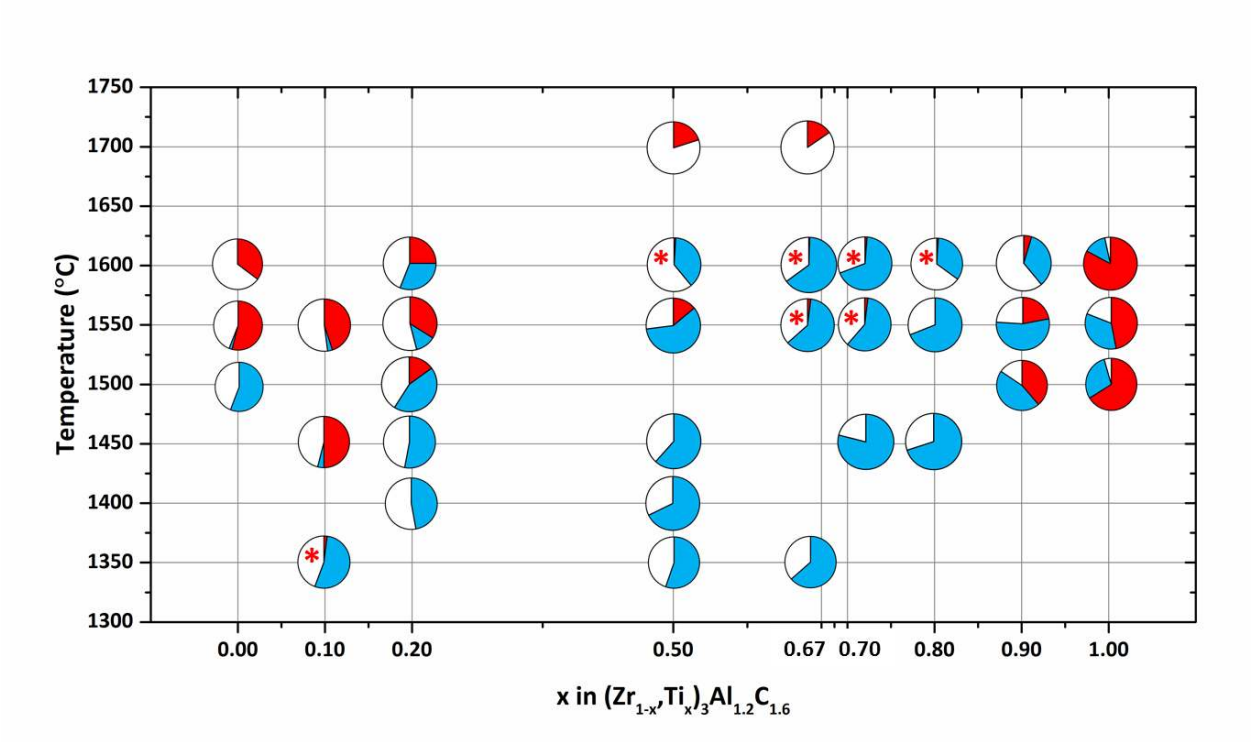

Figure 1. Map showing the phase assembly of MAX phase ceramics synthesized in the Zr-Ti-Al-C system, as a function of the hot-pressing temperature and the Ti content, x, in the $(Zr_{1-x},Ti_x)_3Al_{1.2}C_{1.6}$ starting powder. The phase assembly of the MAX phase ceramics is presented by pie charts where the amount (mass%) of the ZT312 phase appears red, the ZT211 blue, and the secondary phases white. Red stars denote a trace amount of the ZT312 phase.

Certain trends in MAX phase formation can be noticed in **Figure 1**. The ZT211 phase was almost always present in the ceramics hot pressed between 1350°C and 1600°C, except for the low Ti content x=0.1. For this stoichiometry, ZT312 was stable in the 1450-1550°C range, while it was not found at 1450°C in the other stoichiometries. No ZT211 was measured when this stoichiometry was hot pressed at 1500°C and 1550°C, unlike in all other stoichiometries. Therefore, it appears that a small amount of Ti stabilizes the ZT312 phase, which was difficult to form at higher Ti contents. At x=0.67, 0.7 and 0.8, only trace amounts of ZT312 were detected by XRD in the ceramics hot pressed at 1600°C. The maximum total amount of MAX phases (~85 mass% at 1500°C) in the hot pressed Zr-Ti-Al-C ceramics was observed for x=0.9. The XRD results acquired from a whole range of ceramics hot pressed at 1550°C are compared in **Figure 2**, where (Zr,Ti)C and (Ti,Zr)C represents the Zr-rich and Ti-rich ternary carbides, respectively.

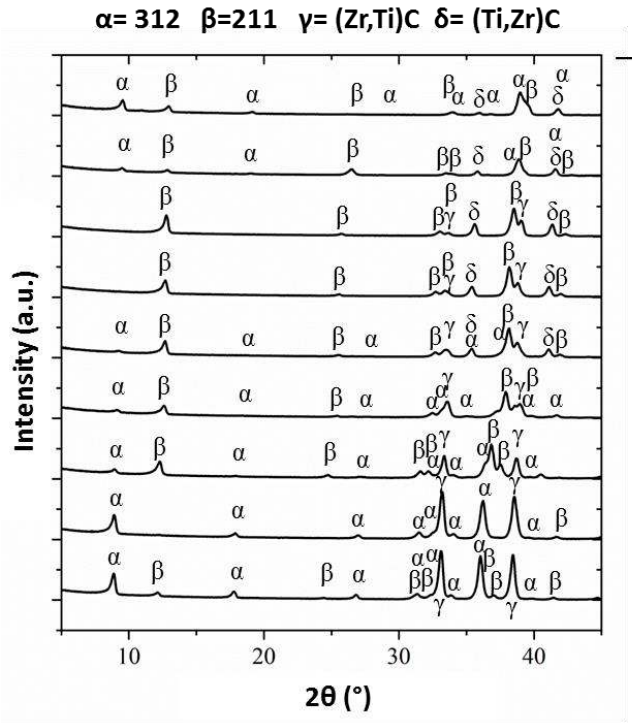

X values	312	211	(Zr,Ti)C	(Ti,Zr)C
1	47(2)	34(1)		TiC=19(1)
0.9	22(1)	54(3)		24(1)
0.8		69(1)		31(1)
0.7	t.a.	60(1)	9(1)	30(1)
0.67	t.a.	62(1)	10(1)	27(1)
0.5	14(1)	59(1)	25(1)	2(1)
0.2	34(1)	12(1)	54(1)	
0.1	45(1)	3(1)	52(1)	
0	54(1)	2(1)	ZrC=44(2)	

Figure 2. XRD patterns and phase assembly in ceramics hot pressed at 1550°C as a function of the $(Zr_{1-x},Ti_x)Al_{1.2}C_{1.6}$ starting powder composition. Numbers in parenthesis indicate the uncertainty in the last digit of mass percentage values.

BSE images of typical microstructures of $(Zr_{0.8},Ti_{0.2})_3Al_{1.2}C_{1.6}$ ceramics hot pressed in the 1400-1500°C range are shown in **Figure 3**. At 1400°C, large $ZrAl_2$ grains (**Figure 3a**) containing fine (Zr,Ti)C grains were observed inside a ZT211 matrix. At 1450°C, the amount of intermetallics decreased and grain growth of the mixed carbides was observed, while the ZT312 phase did not form. At 1500°C, elongated ZT312 grains enveloped by ZT211 grains were observed, and the (Zr,Ti)C grains were dispersed in a mixed ZT211/$ZrAl_2$ matrix.

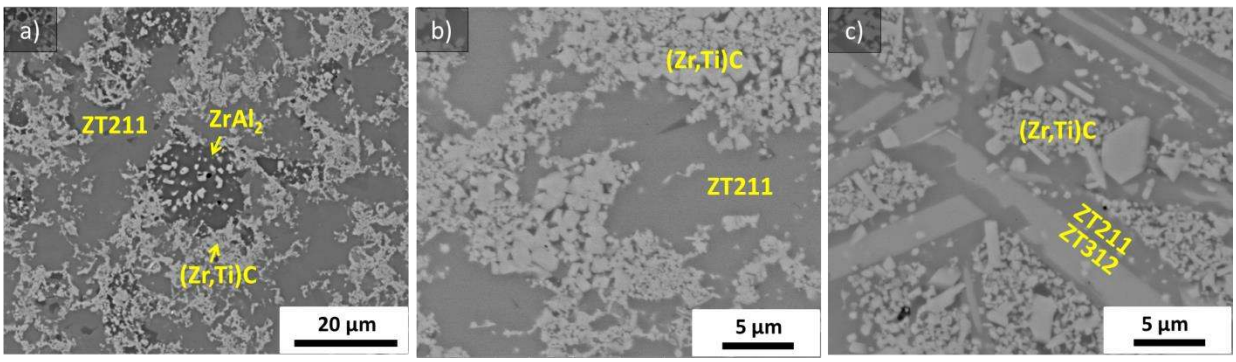

Figure 3. BSE images of $(Zr_{0.8},Ti_{0.2})_3Al_{1.2}C_{1.6}$ ceramics hot pressed at (a) 1400°C, (b) 1450°C, and (c) 1500°C.

3.2. Pressureless MAX phase synthesis. After hot pressing, solidified residues were observed on the die/punch setup, a fact indicating material loss during processing. Possible chemical reactions between intermetallics in the Zr-Al system (Zr_5Al_4, Zr_2Al_3, $ZrAl_2$, $ZrAl_3$) known to result in liquid phase formation are summarised below.[24] During hot pressing, it is possible that liquid products of such reactions might be squeezed into the clearances of the die/punch setup, forming the observed residues.

$$Zr_5Al_4 + Zr_2Al_3 \leftrightarrow L \quad (1477°C)$$
$$Zr_2Al_3 \leftrightarrow ZrAl_2 + L \quad (1592°C)$$
$$ZrAl_2 \leftrightarrow L \quad (1658°C)$$
$$ZrAl_2 + ZrAl_3 \leftrightarrow L \quad (1583°C)$$
$$ZrAl_3 \leftrightarrow L \quad (1583°C)$$
$$Al(FCC) \leftrightarrow L + ZrAl_3 \quad (660°C)$$

As aluminium and its intermetallics are the Al source for MAX phase formation, selected powder mixtures, i.e., $(Zr_{1-x},Ti_x)_3Al_{1.2}C_{1.6}$ with x=0.2, 0.5, 0.9, were pressureless sintered to eliminate liquid-phase losses during processing. Indeed, no significant losses were observed during these tests. Quite interestingly, the amount of secondary Zr-Ti carbides in all pressureless sintered ceramics was lower than in their hot pressed equivalents. **Table 1** summarises the results of Rietveld refinement of the XRD patterns acquired from both hot pressed and pressureless sintered ceramics having the same powder mixture, and gives comparison of the acquired phase assemblies. The lower carbide content can be explained by the more efficient containment of Al and its compounds, which favour potential reactions involving these carbides and leading to MAX phase formation. The amount of Zr_2Al_3 and/or $ZrAl_3$ was higher in the pressureless sintered ceramics. Based on the above, pressureless sintering in the Zr-Ti-Al-C system and its sub-systems should be studied in more detail in the future to improve the phase purity of the produced MAX phase ceramics.

Table 1. Phase assembly of the pressureless sintered and hot pressed ceramics, as obtained by Rietveld refinement of the acquired XRD patterns.

Powder Mixture	T (°C) /	Phase content (mass%)	R_{wp}	R_{exp}

	P (MPa)	ZT211	ZT312	(Zr,Ti)C	(Ti,Zr)C	Zr_2Al_3	$ZrAl_3$	(%)	(%)
$(Zr_{0.8},Ti_{0.2})_3Al_{1.2}C_{1.6}$	1550/30	12(1)	34(1)	54(1)	-	-	-	9.49	2.90
$(Zr_{0.8},Ti_{0.2})_3Al_{1.2}C_{1.6}$	1550/0	55(1)	12(1)	30(1)	-	3(1)	-	11.55	3.09
$(Zr_{0.5},Ti_{0.5})_3Al_{1.2}C_{1.6}$	1700/30	-	18(1)	44(1)	38(1)	-	-	6.56	3.28
$(Zr_{0.5},Ti_{0.5})_3Al_{1.2}C_{1.6}$	1700/0	-	52(1)	27(1)	5(1)	-	16(1)	10.69	3.41
$(Zr_{0.1},Ti_{0.9})_3Al_{1.2}C_{1.6}$	1500/30	46(1)	39(2)	-	15(2)	-	-	10.30	3.93
$(Zr_{0.1},Ti_{0.9})_3Al_{1.2}C_{1.6}$	1500/0	51(1)	39(1)	-	10(1)	-	-	12.87	3.92

3.3. STEM results. Figure 4 shows HAADF STEM images of Zr-Ti-Al-C MAX phases and typical structural anomalies; all STEM images were acquired along the $< 11\bar{2}0 >$ zone axis. **Figures 4a** and **4c** show the $(Zr_{0.8},Ti_{0.2})_3Al_{1.2}C_{1.6}$ ceramic hot pressed at 1500°C. 211 stackings (**Figure 4a**) and alternating 211 and 312 stackings that create a local 523 structure within a ZT312 grain (**Figure 4c**) were observed. 523 peaks could not be identified in the XRD spectra, since the 523 stackings are believed to represent a small material fraction that might have resulted from local transformations between the ZT211 and ZT312 phases. Similar observations have been made for MAX phases in the Hf-Al-C system.[25] **Figures 4b**, **4d** and **4e** show the $(Zr_{0.5},Ti_{0.5})_3Al_{1.2}C_{1.6}$ ceramic pressureless sintered at 1700°C. This sample was selected for detailed TEM analysis, due to the relatively high (~52 mass%) ZT312 content (**Figure 4b**). Apart from the observed mixed stackings, "zipper"-like stacking faults were also observed (**Figures 4d-4e**), where MX layers within the same MAX phase unit cell merge into a single band of similar or larger thickness at different locations. The "zipper"-like features can be a consequence of the transition from the ZT211 to the ZT312 phase by the outward diffusion of Al, the inward diffusion of C and the local re-adjustment of the M layers, as has been earlier proposed for the Hf-Al-C MAX phases.[25] An evidence of this proposed transition can also be found in SEM images of ZT312 and ZT211 mixtures (**Figure 3c**), where the ZT312 grains are surrounded by ZT211 grains, supporting the possibility of a phase transition within the ZT211 grain. These structural anomalies were observed at the boundaries between areas with different Ti/Zr ratios, as shown in **Figures 4d-4e**, where Ti-rich (darker) and Zr-rich (brighter) regions appear to converge at the locations of the defect-rich boundaries.

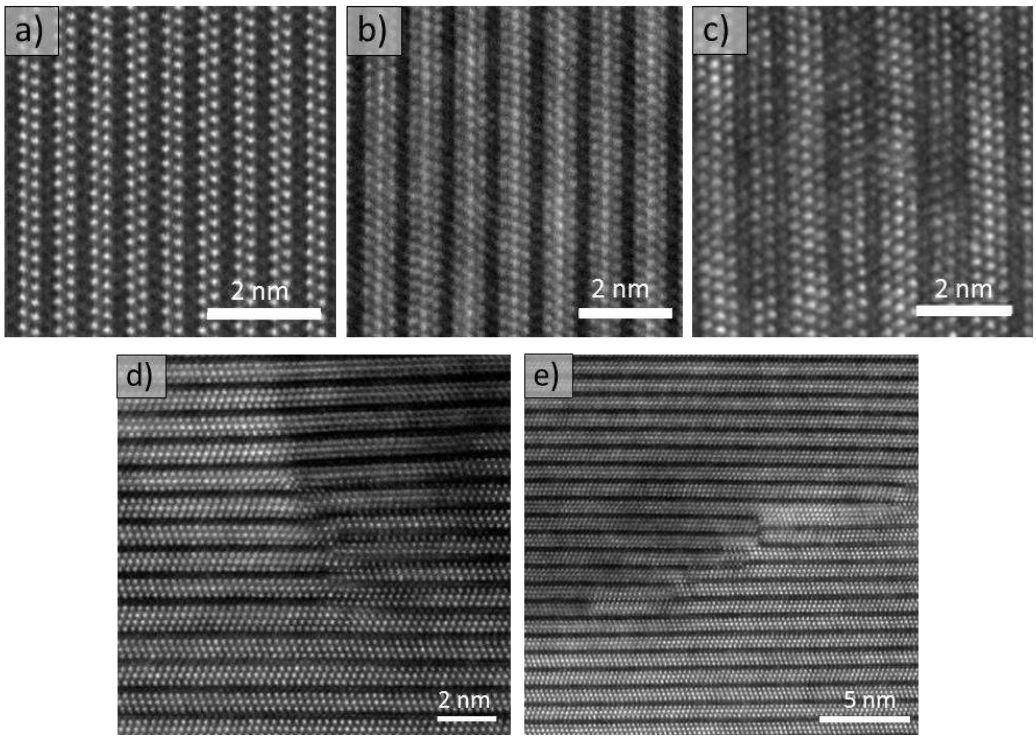

Figure 4. HAADF STEM images along the $< 11\bar{2}0 >$ zone axis of MAX phase grains. (a) 211 and (c) 523 stackings in the $(Zr_{0.8},Ti_{0.2})_3Al_{1.2}C_{1.6}$ ceramic hot pressed at 1500°C. (b) 312 stackings and (d-e) "zipper"-like stacking faults within a ZT312 grain in the $(Zr_{0.5},Ti_{0.5})_3Al_{1.2}C_{1.6}$ ceramic pressureless sintered at 1700°C. Stacking faults outline the boundaries between areas with different Ti/Zr ratios, as indicated by differences in the local compositional contrast.

Variations in the local chemical composition were mapped by EDS and results are presented in **Figure 5**. Areas marked as 1 and 2 had ~55 at% and ~47 at% Ti, respectively. Scanning areas situated further apart showed that the composition could vary from ~78 at% to 50 at% Ti within the same grain. Similar variations in composition were also identified within (Zr,Ti)C grains. Although the presence of these stacking faults at the boundaries between zones with different compositions cannot yet be explained, it could be tentatively attributed to the lattice mismatch between zones with different compositions.

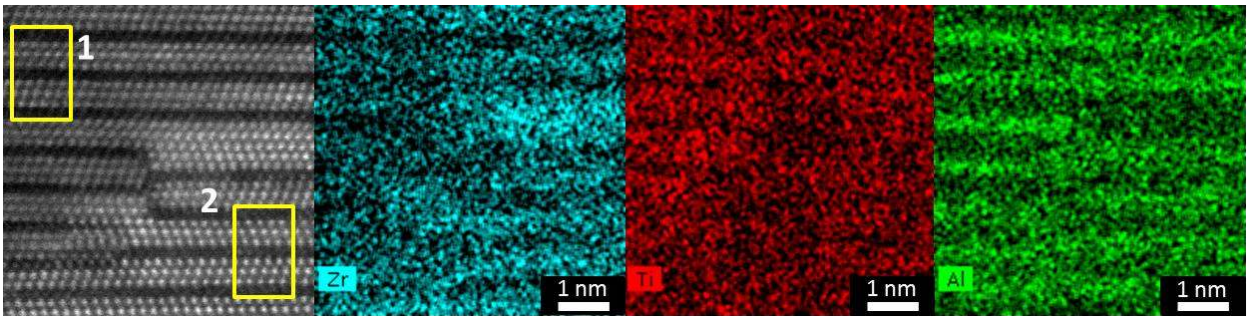

Figure 5. HAADF STEM image and EDS maps for Zr, Ti and Al showing compositional non-uniformities within the same ZT312 grain.

3.4. Rietveld refinement results. The lattice parameters, *a* and *c*, were obtained by Rietveld refinement and are listed in **Table 2**, which also includes the literature data for the Zr- and Ti-based end members. **Figures 6a and 6b** show the refined lattice parameters for ZT211 and ZT312 as a function of the Ti content, x, in the starting powder. Ideally, the lattice parameters should have been plotted versus the exact Ti content of the phases. Due to the non-uniform Zr and Ti distribution in the MAX grains (**Figures 4 and 5**), local variations in lattice parameters should also be expected. This was supported by XRD analysis and by the observed broadening of MAX phase peaks. Peak broadening was also seen in other solid solution MAX phases.[26] For these reasons, the representation of the acquired results (**Figure 6**) does not take into account the non-uniform distribution of Ti/Zr, and the Ti content of the starting powder was used instead. For the ZT211 phase, SEM EDS point measurements confirmed that the amount of Ti inside the MAX phases was close to the initially added Ti amount, except for the ceramic with x=0.5. Within this particular ceramic, grains with a higher Ti content (x≈0.7) were found. This could explain the deviation from the linear trend at x=0.5 in **Figure 6a**; the observed overall agreement with linearity confirms that the ZT211 ceramics obey Vegard's law for solid solutions.[27] For the ZT312 phase, the linear fit was plotted using literature data for the lattice parameters of Zr_3AlC_2 and Ti_3AlC_2 (**Figure 6b**). Although the decreasing trend for *a* is confirmed for ZT312, the linear fit between end members offers only a rough approximation. From all data points, the one corresponding to 0.67 Ti deviates the most from such trend. Whether one should analyse it as an outlier or a break point in the trend remains to be seen, but it might not be a coincidence that it corresponds to the composition where the Ti:Zr ratio (2:1) corresponds to a fully-ordered structure. This local deviation from linearity around 0.67 Ti can be attributed to the effect of Zr and Ti ordering on the ZT312 lattice parameters, as proposed in the following section.

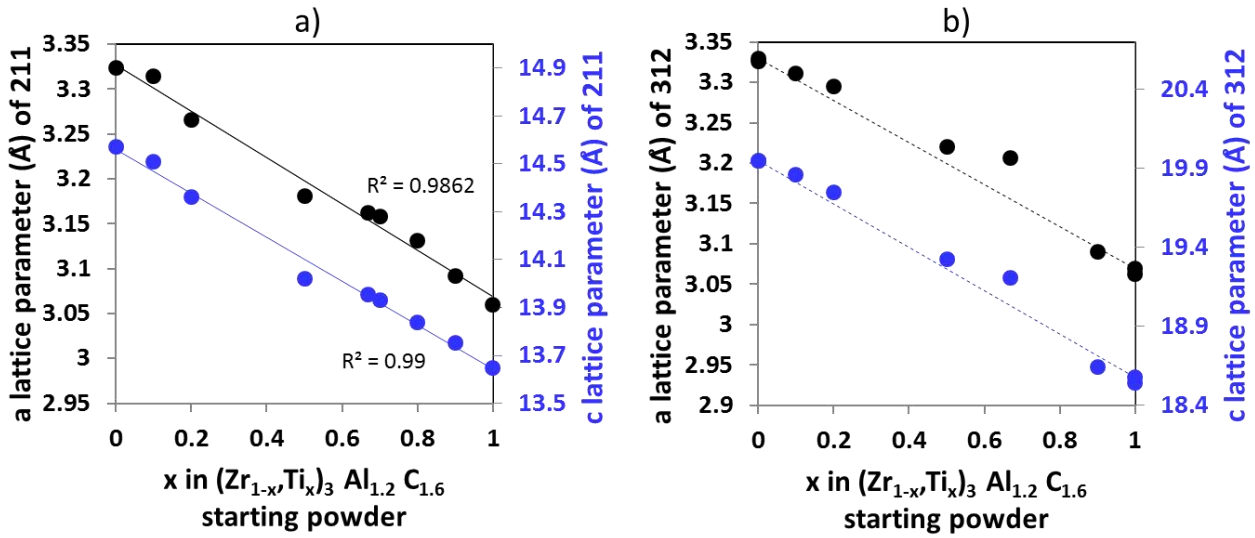

Figure 6. Lattice parameters of the ZT211 (a) and ZT312 (b) MAX phases obtained by Rietveld refinement of the XRD spectra of the produced ceramics, as a function of the Ti content, x, in the starting powder.

Table 2. Refined lattice parameters of the ZT211 and ZT312 MAX phases, as determined by Rietveld analysis of XRD data. Refinement was done using the P63/mmc space group with the following atomic positions: for ZT211, (Zr_{1-x},Ti_x) at 4f(2/3, 1/3, z~0.08), Al at 2c(1/3, 2/3, 1/4), and C at 2a(0, 0, 0); for ZT312, $(Zr_{1-x},Ti_x)1$ at 4f(1/3, 2/3, z~0.132), $(Zr_{1-x},Ti_x)2$ at 2a(0, 0, 0), Al at 2b(0, 0, 1/4), and C at 4f(2/3, 1/3, z~0.07).

	0[6,7]	**0**†	**0.1**†	**0.2**†	**0.5**†	**0.67**†	**0.7**†	**0.8**†	**0.9**†	**1**†	**1**[1,4]
312 *a* (Å)	3.33308(6)	3.3263(4)	3.3106(3)	3.2938(3)	3.220(1)	3.206(1)			3.0897(3)	3.0624(6)	3.07
312 *c* (Å)	19.9507(3)	19.947(3)	19.836(2)	19.755(3)	19.325(9)	19.209(2)			18.641(3)	18.544(2)	18.58
211 *a* (Å)	3.3237(2)	3.323(2)	3.314(3)	3.2656(5)	3.1813(1)	3.1627(2)	3.1583(1)	3.1314(2)	3.0919(2)	3.0596(4)	3.04
211 *c* (Å)	14.5705(5)	14.570(3)	14.507(7)	14.363(3)	14.0204(9)	13.9534(9)	13.9307(9)	13.8381(8)	13.750(1)	13.647(2)	13.60
R_{wp} (%)		16.8	11.42	9.5	8.86	10.82	8.79	12.63	10.26	15.44	
R_{exp} (%)		2.96	2.93	2.89	3.5	3.56	3.41	3.51	4.58	4.13	

† These stoichiometries were studied in the framework of this work.
A hexagonal crystal structure with space group P63/mmc was assumed for both ZT211 and ZT312 MAX phases.
Numbers in parenthesis indicate uncertainty in the last digit.

3.5. Ordering of Zr and Ti in ZT312 and ZT413 MAX phases. As possible cause for the deviation from Vegard's law, the potential Zr and Ti atomic ordering in ZT312 MAX phases at x=0.67 (i.e., $(Zr_{0.33},Ti_{0.67})_3AlC_2$ or $ZrTi_2AlC_2$ stoichiometry) was studied by simulating the unit cell and comparing the experimental XRD peak intensities to the simulated ones. The

effect of preferred orientation, i.e., texture, on the peak intensities was neglected, since the XRD spectra were acquired from powder samples. In the ZT312 unit cell, it is important to note that Zr and Ti elements can occupy two different crystallographic sites (M1 at position 4f (1/3, 2/3, z~0.132), close to the A-layers, and M2 at position 2a(0, 0, 0)), in the middle of the octahedra layers. The unit cell was here modified to have different Ti occupancies in the M1 site, whereas M2 sites were occupied only by Zr atoms. **Figure 7** shows the evolution in the XRD peak intensities when the structure becomes progressively fully ordered (transition from black dot to blue dot), i.e., the evolution from Ti=0 (Zr_3AlC_2) to Ti=1 (fully-ordered $ZrTi_2AlC_2$) on the M1 site. **Figure 8** compares simulated and experimental XRD intensities for the ZT312 phase in the $(Zr_{0.5},Ti_{0.5})_3Al_{1.2}C_{1.6}$ ceramic sintered at 1700°C. Only the refined ZT312 intensities are plotted from the experimental XRD data, while the theoretical peak intensities of Zr_3AlC_2, Ti_3AlC_2 and disordered $(Zr_{0.5},Ti_{0.5})_3AlC_2$ phases are added for comparison. The comparison of XRD peak intensities was done by normalising intensities to the one of the (014) diffraction peak. In order to evaluate only the evolution of the XRD peak intensities, the lattice parameters were kept constant during simulation, despite the fact the 2θ values were also expected to shift when the element occupancy changed. The intensity trend, indicated by arrows for the main peaks in **Figure 7**, agreed with the changes occurring in the simulated XRD patterns (**Figure 8**), implying that ordering presumably occurred in the ZT312 phase.

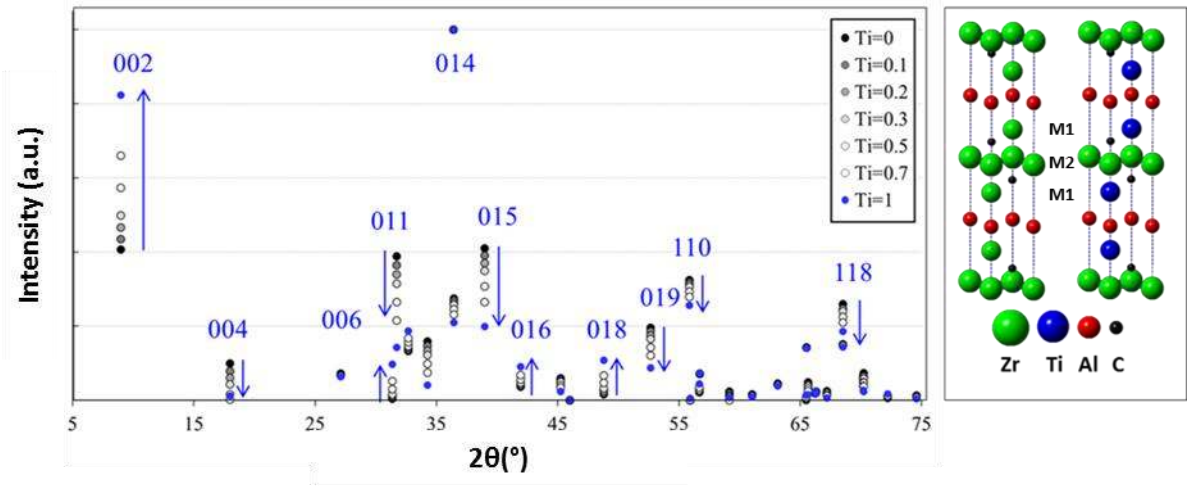

Figure 7. Simulated XRD patterns of the ZT312 structure with changing Ti occupancies on the M1 site (1/3, 2/3, 0.1324). The arrows show the change in XRD peak intensity as the structure becomes progressively ordered. The idealised unit cells on the right depict pure Zr_3AlC_2 and ordered $(Zr_{0.33},Ti_{0.67})_3AlC_2$.

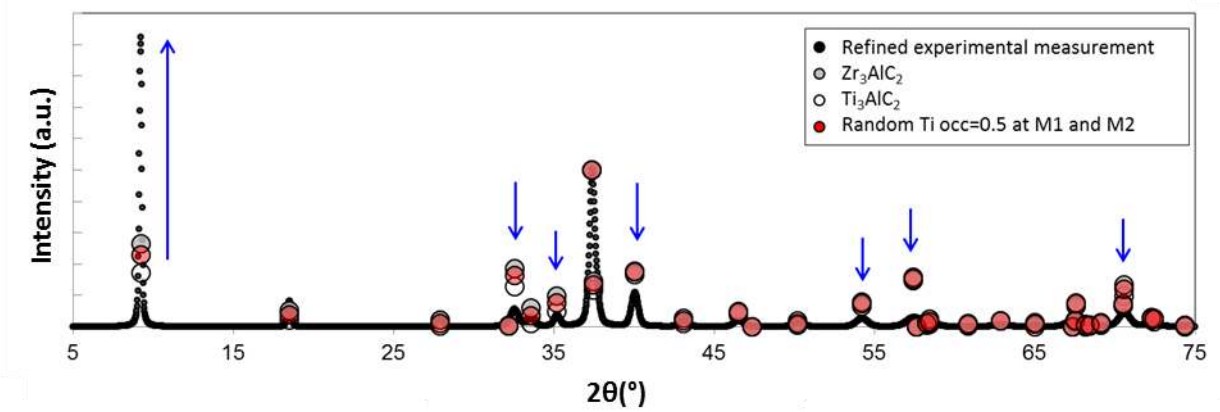

Figure 8. Theoretical XRD peak intensities of Zr_3AlC_2, Ti_3AlC_2, and $(Zr,Ti)_3AlC_2$ with a Ti occupancy of 0.5 at both M1 and M2 sites, as compared with the refined peak intensities of the ZT312 phase in the $(Zr_{0.5},Ti_{0.5})_2Al_{1.2}C_{1.6}$ ceramic sintered at 1700°C.

The STEM/EDS results in **Figures 9a** and **9b** also confirm that heavier Zr atoms preferentially position themselves in the middle layer of the ZT312 structure, while Ti atoms are dominant in the outer layers, creating a 'sandwich'-like ordered structure. The Ti profile shows a plateau over all three M layers. Note that the limited EDS resolution did not allow the deconvolution of the Ti peaks into their individual components in the three M layers. Since brightness in the HAADF STEM images increases with the atomic mass, average intensity profiles were plotted (**Figures 9b** and **9c**). The intensity profiles indicate atomic ordering in the M layers. When the intensity profile of **Figure 9c** is examined in detail, ordering is easily recognized on the left side of the image. The contrast difference between different M layers (M2-middle layer and M1-outer layers) decreases towards the right, showing a gradual change in ordering and possibly in composition. In the 413 stacking (blue frame in **Figure 9c**) found within ZT312, the two central rows appear brighter, suggesting enrichment in the heavier Zr. Similar intensity profiles were measured in 413 bands found in other ZT312 grains (not shown here), suggesting that ordering in ZT413 is a fact.

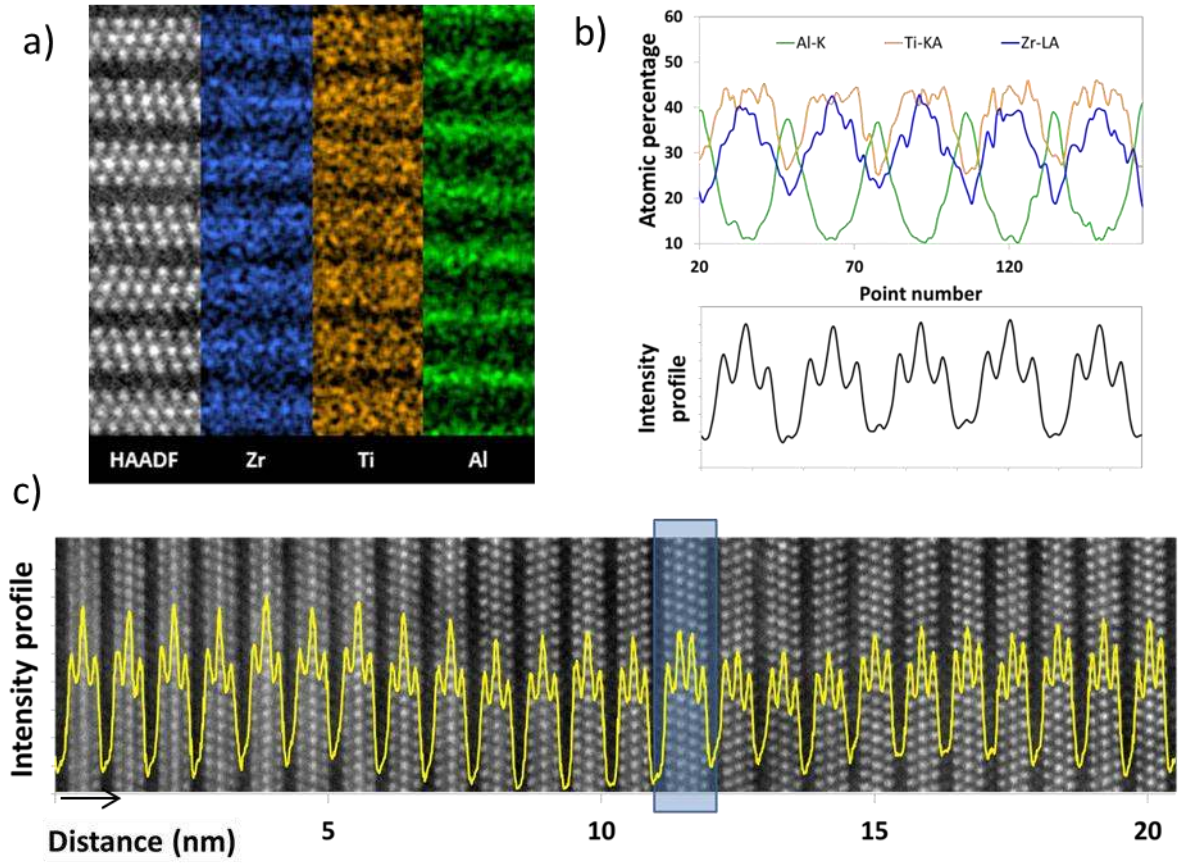

Figure 9. (a-b) STEM/EDS results acquired from a $(Zr_{0.5},Ti_{0.5})_3Al_{1.2}C_{1.6}$ ceramic pressureless sintered at 1700°C indicate Zr enrichment in the central M-site of the ZT312 phase. (c) An average intensity profile reveals ordering in the vertical atomic rows and a bluish frame highlights a local 413 stacking.

So far, five ordered MAX phases have been experimentally observed in three quaternary systems: Cr_2VAlC_2 and $Cr_2V_2AlC_3$,[28] Cr_2TiAlC_2,[12,27] Mo_2TiAlC,[29] and $Mo_2Ti_2AlC_3$.[30] In these MAX phases, elements from group VI (Cr and Mo) were located in the M1-site that is connected to the A-layer, while elements from groups IV & V (i.e., Ti and V, respectively) were located in the middle of the M_6X layers.

Theoretical studies on ordering in MAX phases have been carried out using computational tools. A first set of ordered, double transition metal carbides was studied in relation with MAX phase-derived two-dimensional materials known as MXenes. Anasori et al. predicted a set of 24 stable ordered MXene structures based on DFT-calculations;[31] however, the Zr-Ti-Al-C system was not included in these calculations. More recently, Dahlqvist et al. evaluated order and disorder in TiMAlC, TiM_2AlC_2, MTi_2AlC_2, and $Ti_2M_2AlC_3$ where Zr was included

in the M elements.[32] The calculated formation enthalpy (ΔH_{cp}) values for the relevant MAX phases (TiZrAlC, $TiZr_2AlC_2$, $ZrTi_2AlC_2$ and $Ti_2Zr_2AlC_3$) were predicted by these authors to be more positive compared to the competing phases, suggesting that MAX phases were unlikely to form in these systems. However, our experimental data demonstrate the opposite. On the other hand, when looking at the most stable ordered configurations, certain agreements can be found between theory and experiments. The predicted as most stable structures, i.e., structures with the lowest ΔH_{cp} at 0 K, for TiZrAlC (disordered), $ZrTi_2AlC_2$ (ordered with Ti on M1-site) and $Ti_2Zr_2AlC_3$ (ordered with Ti on M1-site) match with the experimentally observed atomic stackings. For the $TiZr_2AlC_2$ stoichiometry, no clear indication of atomic ordering was experimentally observed, but also here a preferred occupancy of the M1-site by Ti atoms is not excluded.

Two main factors responsible for ordering were already addressed by Hume-Rothery: a clear difference in electronegativity (χ) and in covalent radii.[33] Both differences are significant for the Ti-Zr pair and could account for the particular ordering in the Zr-Ti-Al-C system, where Ti occupies preferentially the M1-site, while Ti occupies preferentially the M2-site in the other ordered systems. For both factors, the ordering is consistent in all ordered MAX phases so far reported. It appears that the M-element with the smallest atomic radius (Cr < V < Mo < Ti < Zr) and the highest electronegativity (Mo > Cr > V > Ti > Zr) is positioned in the outer-layers of the M1-M2-M1 'sandwich' (312-structure) or M1-M2-M2-M1 'sandwich' (413-structure) next to the A-element layer, whereas the larger and less electronegative M-element is positioned inside the 'sandwich' structure on the M2-sites. It is difficult to identify the most dominant factor of the two, as the trends for the electronegativity and the atomic radius are exactly opposite. It can, however, be mentioned that in some cases the difference in electronegativity is limited (i.e., $\Delta\chi$ for V and Cr is 0.03, corresponding to <2% change in χ(Cr)), while the difference in atomic radii is invariably significant (>8%). Considering this steric-based hypothesis, one might suggest that smaller M-atoms form more stable bonds with small A-atoms (e.g., Al tends to form more stable bonds with Ti than with Zr), thus forming more compact triangular prisms.

As opposed to other ordered MAX phases, such as $Mo_2Ti_2AlC_3$ or Mo_2TiAlC_2,[30] $(Zr,Ti)_3AlC_2$ has a gradually changing lattice parameter as a function of the amount of Ti substituting Zr (**Figure 6b**). Formation of ZT312, not only for the ordered stoichiometry but also within a range of stoichiometries, indicates that ZT312 can be obtained in a solid solution form or as an ordered quaternary MAX phase.

3.6. Secondary phases. A bimodal grain size distribution was observed for the (Zr,Ti)C carbides, i.e., a combination of significantly larger (>2 μm) and submicrometre-size grains (see **Figure 3**). It should be noted that the grain size of these mixed carbides is well below the grain size of the initial TiH_2 and ZrH_2 powders. The angular morphology of the (Zr,Ti)C carbides indicates that they might have precipitated from a liquid phase rather than formed by solid state diffusion. Fine-grained ZrC synthesis was also reported during a self-propagating reaction in elemental Al-Zr-C powder mixtures.[34]

Formation of secondary phases was also observed in interrupted pressureless sintered ceramics made from a $(Zr_{0.8},Ti_{0.2})_3Al_{1.2}C_{1.6}$ starting powder heated at the same rate as the hot pressed ceramics. When heated to 625°C, i.e., below the melting temperature of Al (660°C), for 5 minutes and immediately furnace cooled, the ceramic contained only about 3 mass% elemental Al (**Table 3**). The amount of elemental Al was comparable after a similar treatment at 675°C, while the Al content in the initial powder mixture was 10.6 mass%. This indicates that Al reacts to form intermetallics even below its melting point. The presence of substantial amounts of $ZrAl_3$ and especially $ZrAl_2$ (**Table 3**) was confirmed by XRD and Rietveld refinement results.

Formation of ZrC was observed in the powder mixture heated to 675°C, but not in the one heated to 625°C. These results indicate that the coarse (Zr,Ti)C grains observed in the hot pressed ceramics might have already formed during the heating stage between 625-675°C. The lattice parameter of ZrC was close to the literature value of 4.683 Å,[35] indicating no (or a very small amount) of Ti in solid solution at such low temperatures. The ZrH_2 and TiH_2 starting powders dehydrogenated during heating and no residual peaks of these phases were identified.

Table 3. Rietveld refinement results of XRD data from interrupted pressureless sintering runs.

T (°C)	Powder Mixture	Zr (mass%)	Al (mass%)	C (mass%)	ZrC (mass%)	$ZrAl_3$ (mass%)	$ZrAl_2$ (mass%)	R_{wp} (%)	R_{exp} (%)
625	$(Zr_{0.8},Ti_{0.2})_3Al_{1.2}C_{1.6}$	43(2)	3(1)	17(1)	0	7(1)	29(1)	16.69	2.86
675	$(Zr_{0.8},Ti_{0.2})_3Al_{1.2}C_{1.6}$	37(1)	3(1)	11(1)	27(1)	4(1)	17(1)	11.75	4.04

With a Ti content in the starting powder of ≥25 at% (≥ x=0.5) at the low temperature of 1350°C, only one set of XRD peaks was observed belonging to a single mixed carbide. For ceramics hot pressed at temperatures ≥1450°C, two distinct sets of peaks were observed in

the XRD patterns belonging to two ternary mixed (Zr,Ti)C carbides, one rich in Zr and the other rich in Ti. This was interpreted as the decomposition of the mixed carbides with the increase in temperature. The lattice parameters of the Zr-rich and Ti-rich carbides are plotted in **Figure 10**, indicating the phase separation. Taking into account the miscibility gap in the ZrC-TiC system,[36] the decomposition of mixed carbides is not surprising. Although the calculated temperatures for the miscibility gap are very high (~2000 K), simulation studies suggested that carbon vacancies in the mixed (Zr,Ti)C carbides account for significant deviations in the onset temperature of phase separation.[37] The onset of immiscibility was shown to occur at lower temperatures as the amount of C vacancies in the mixed carbide increased. The separation temperatures in the performed simulations for 20% C vacancies are very similar to the experimental processing temperatures in this work, but the extent of the C sub-stoichiometry was not systematically analysed.

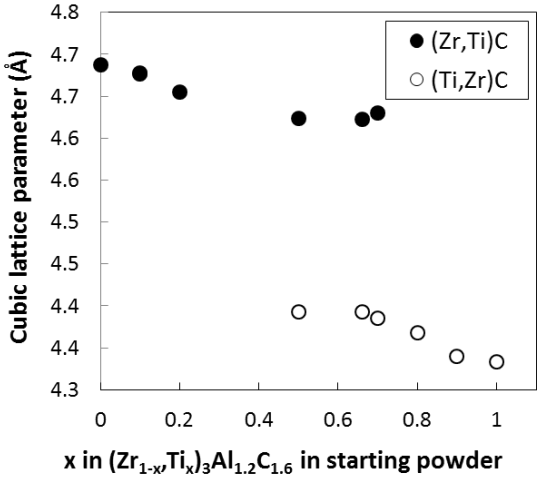

Figure 10. Cubic lattice parameter of mixed Zr-Ti carbides as a function of the starting powder composition of the hot pressed ceramics.

4. CONCLUSIONS

ZT211 and ZT312 MAX phase solid solutions have been synthesized in the Zr-Ti-Al-C system by reactive hot pressing, as well as by pressureless sintering of ZrH_2, TiH_2, Al and C powder mixtures. $(Zr_{1-x},Ti_x)_3Al_{1.2}C_{1.6}$ starting powder stoichiometries with x=0-1 were investigated. Ti was found to substitute Zr in Zr_2AlC and Zr_3AlC_2 phases to form $(Zr,Ti)_2AlC$ and $(Zr,Ti)_3AlC_2$ solid solutions over the complete compositional range. HAADF STEM

imaging combined with EDS revealed ordering of the Ti and Zr atoms in ZT312, with the Zr atoms 'sandwiched' between two Ti layers in the M_6C structure. Atomic ordering similar to that observed in ZT312 was also observed in ZT413 bands, with the two middle layers (M2 position) showing a higher Zr content 'sandwiched' again between two Ti layers (M1 position). The ordering was also supported by the comparison of simulated and experimental XRD spectra. HRSTEM examination of ZT211 and ZT312 showed that a mixture of 211-312 (523) and 413 stackings can be present inside a single grain, suggesting a transition from one MAX phase to another. Decomposition of the mixed (Zr,Ti)C secondary phases into Zr-rich and Ti-rich carbide mixtures was observed upon sintering in the 1350-1700°C range, in agreement with the existing miscibility gap in the ZrC-TiC system. This decomposition was noticed for $(Zr_{1-x},Ti_x)_3Al_{1.2}C_{1.6}$ stoichiometries with $x \geq 0.5$. Pressureless sintering was found to be an alternative method of MAX phase synthesis in the Zr-Ti-Al-C system that resulted in a higher MAX phase content and less secondary carbides as compared to the hot pressed ceramic equivalents, probably due to reduced liquid-phase losses. Further optimization of the processing steps is still required to obtain ceramics of high phase purity in this MAX phase system.

AUTHOR INFORMATION

Corresponding Author

*Email: btunca@sckcen.be

Notes

The authors declare no competing financial interest.

ACKNOWLEDGEMENTS

The presented research was partly funded by the European Atomic Energy Community's (Euratom) Seventh Framework Programme FP7/2007-2013 under Grant Agreement No. 604862 (FP7 MatISSE) and falls within the framework of the EERA (European Energy Research Alliance) Joint Programme on Nuclear Materials (JPNM). T. Lapauw thanks the Agency for Innovation by Science and Technology (IWT), Flanders, Belgium, for PhD Grant No. 131081. B. Tunca acknowledges the financial support of the SCK•CEN Academy for Nuclear Science and Technology. The authors acknowledge the Fund for Scientific Research

Flanders (FWO-Vlaanderen) under Grant G.0431.10N.F. and the Hercules Foundation under Project ZW09-09 and AKUL/1319 (CombiS(T)EM).

REFERENCES

(1) Jeitschko, W.; Nowotny, H.; Benesovsky, F. Kohlenstoffhaltige Ternaire Verbindungen (H-Phase). *Monatshefte für Chemie* **1963**, *332*, 2–6.

(2) Barsoum, M. W.; El-Raghy, T. Synthesis and Characterization of a Remarkable Ceramic: Ti_3SiC_2. *J. Am. Ceram. Soc.* **1996**, 79, 1953-1956.

(3) Barsoum, M. W. The $M_{n+1}AX_n$ Phases : A New Class of Solids. *Prog. Solid State Chem.* **2000**, *28*, 201–281.

(4) Barsoum, M. W. MAX Phases Properties of Machinable Ternary Carbides and Nitrides; Wiley -VCH Verlag GmbH & Co. KGaA, **2013**, 1.

(5) Tallman, D. J.; Anasori, B.; Barsoum, M. W. A Critical Review of the Oxidation of Ti_2AlC, Ti_3AlC_2 and Cr_2AlC in Air. *Mater. Res. Lett.* **2013**, *1*, 115–125.

(6) Lapauw, T.; Lambrinou, K.; Cabioc'h, T.; Halim, J.; Lu, J.; Pesach, A.; Rivin, O.; Ozeri, O.; Caspi, E. N.; Hultman, L.; Eklund, P.; Rosén, J.; Barsoum, M. W.; Vleugels, J. Synthesis of the New MAX Phase Zr_2AlC. *J. Eur. Ceram. Soc.* **2016**, *36*, 1847–1853.

(7) Lapauw, T.; Halim, J.; Lu, J.; Cabioc'h, T.; Hultman, L.; Barsoum, M. W.; Lambrinou, K.; Vleugels, J. Synthesis of the Novel Zr_3AlC_2 MAX Phase. *J. Eur. Ceram. Soc.* **2016**, 36, 943-947.

(8) He, L. F.; Bao, Y. W.; Li, M. S.; Wang, J. Y.; Zhou, Y. C. Oxidation of $Zr_2[Al(Si)]_4C_5$ and $Zr_3[Al(Si)]_4C_6$ in Air. *J. Mater. Res.* **2008**, *23* , 3339–3346.

(9) Lu, X.; Xiang, H.; He, L.-F.; Sun, L.; Zhou, Y. Effect of Ti Dopant on the Mechanical Properties and Oxidation Behavior of $Zr_2[Al(Si)]_4C_5$ Ceramics. *J. Am. Ceram. Soc.* **2011**, *94*, 1872–1877.

(10) Wan, D. T.; He, L. F.; Zheng, L. L.; Zhang, J.; Bao, Y. W.; Zhou, Y. C. A New Method to Improve the High-Temperature Mechanical Properties of Ti_3SiC_2 by Substituting Ti with Zr, Hf, or Nb. *J. Am. Ceram. Soc.* **2010**, *93*, 1749–1753.

(11) Liu, Z.; Wu, E.; Wang, J.; Qian, Y.; Xiang, H.; Li, X.; Jin, Q.; Sun, G.; Chen, X.; Wang, J.; Li, M. Crystal Structure and Formation Mechanism of $(Cr_{2/3}Ti_{1/3})_3AlC_2$ MAX Phase. *Acta Mater.* **2014**, *73*, 186–193.

(12) Horlait, D.; Grasso, S.; Chroneos, A.; Lee, W. E. Attempts to Synthesise Quaternary MAX Phases $(Zr,M)_2AlC$ and $Zr_2(Al,A)C$ as a Way to Approach Zr_2AlC. *Mater. Res.*

Lett. **2016**, *3831*, 1–8.

(13) Hadi, M. A.; Panayiotatos, Y.; Chroneos, A. Structural and Optical Properties of the Recently Synthesized $(Zr_{3-x}Ti_x)AlC_2$ MAX Phases. *J. Mater. Sci. Mater. Electron.* **2016**, 1–8.

(14) Schuster, J. C.; Nowotny, H.; Vaccaro, C. The Ternary Systems: CrAlC, VAlC, and TiAlC and the Behavior of H-Phases (M_2AlC). *J. Solid State Chem.* **1980**, *32*, 213–219.

(15) Nowotny, H.; Rogl, P.; Schusters, J. C. Structural Chemistry of Complex Carbides and Related Compounds*. *J. Solid State Chem.* **1982**, *4*, 126–133.

(16) Yeh, C. L.; Yang, W. J. Formation of MAX Solid Solutions $(Ti,V)_2AlC$ and $(Cr,V)_2AlC$ with Al_2O_3 Addition by SHS Involving Aluminothermic Reduction. *Ceram. Int.* **2013**, *39*, 7537–7544.

(17) Barsoum, M. W.; Salama, I.; El-Raghy, T.; Golczewski, J.; Seifert, H. J.; Aldinger, F.; Porter, W. D.; Wang, H. Thermal and Electrical Properties of Nb_2AlC, $(Ti, Nb)_2AlC$ and Ti_2AlC. *Metall. Mater. Trans. A* **2002**, *33*, 2775–2779.

(18) Naguib, M.; Bentzel, G. W.; Shah, J.; Halim, J.; Caspi, E. N.; Lu, J.; Hultman, L.; Barsoum, M. W. New Solid Solution MAX Phases: $(Ti_{0.5},V_{0.5})_3AlC_2$, $(Nb_{0.5},V_{0.5})_2AlC$, $(Nb_{0.5},V_{0.5})_4AlC_3$ and $(Nb_{0.8},Zr_{0.2})_2AlC$. *Mater. Res. Lett.* **2014**, *2*, 233–240.

(19) Gu, J.; Pan, L.; Yang, J.; Yu, L.; Zhang, H.; Zou, W.; Xu, C. Mechanical Properties and Oxidation Behavior of Ti-Doped Nb_4AlC_3. *J. Eur. Ceram. Soc.* **2016**, *36*, 1001–1008.

(20) Yang, J.; Naguib, M.; Ghidiu, M.; Pan, L.-M.; Gu, J.; Nanda, J.; Halim, J.; Gogotsi, Y.; Barsoum, M. W. Two-Dimensional Nb-Based M_4C_3 Solid Solutions (MXenes). *J. Am. Ceram. Soc.* **2016**, *99*, 660–666.

(21) Lapauw, T.; Tytko, D.; Vanmeensel, K.; Huang, S.; Choi, P.-P.; Raabe, D.; Caspi, E. N.; Ozeri, O.; to Baben, M.; Schneider, J. M.; Lambrinou, K.; Vleugels, J. $(Nb_X, Zr_{1-X})_4AlC_3$ MAX Phase Solid Solutions: Processing, Mechanical Properties, and Density Functional Theory Calculations. *Inorg. Chem.* **2016**, *55*, 5445–5452.

(22) Lutterotti, L.; Matthies, S.; Wenk, H.-R.; Schultz, A. S.; Richardson, J. W. Combined Texture and Structure Analysis of Deformed Limestone from Time- of - Flight Neutron Diffraction Spectra. *J. Appl. Phys.* **1997**, *81*, 594–600.

(23) Kraus, W.; Nolzeb, G.; IUCr. POWDER CELL – a Program for the Representation and Manipulation of Crystal Structures and Calculation of the Resulting X-Ray Powder Patterns. *J. Appl. Crystallogr.* **1996**, *29*, 301–303.

(24) Wang, T.; Jin, Z.; Zhao, J.-C. Thermodynamic Assessment of the Al - Zr Binary System. *J. Phase Equilibria Diffus.* **2001**, *22*, 544–551.

(25) Lapauw, T.; Tunca, B.; Cabioc'h, T.; Lu, J.; Persson, P. O. Å.; Lambrinou, K.; Vleugels, J. Synthesis of MAX Phases in the Hf–Al–C System. *Inorg. Chem.* **2016**, *55*, 10922–10927.

(26) Cabioc'h, T.; Eklund, P.; Mauchamp, V.; Jaouen, M. Structural Investigation of Substoichiometry and Solid Solution Effects in $Ti_2Al(C_x,N_{1-x})_y$ Compounds. *J. Eur. Ceram. Soc.* **2012**, *32*, 1803–1811.

(27) Vegard, L. Die Konstitution Der Mischkristalle Und Die Raumfüllung Der Atome. *Zeitschrift für Phys.* **1921**, *5*, 17–26.

(28) Caspi, E. N.; Chartier, P.; Porcher, F.; Damay, F.; Cabioc'h, T. Ordering of (Cr,V) Layers in Nanolamellar $(Cr_{0.5},V_{0.5})_{n+1}AlC_n$ Compounds. *Mater. Res. Lett.* **2015**, *3*, 100–106.

(29) Anasori, B.; Halim, J.; Lu, J.; Voigt, C. A.; Hultman, L.; Barsoum, M. W. Mo_2TiAlC_2: A New Ordered Layered Ternary Carbide. *Scr. Mater.* **2015**, *101*, 5–7.

(30) Anasori, B.; Dahlqvist, M.; Halim, J.; Moon, E. J.; Lu, J.; Hosler, B. C.; Caspi, E. N.; May, S. J.; Hultman, L.; Eklund, P.; Rosén, J.; Barsoum, M. W. Experimental and Theoretical Characterization of Ordered MAX Phases Mo_2TiAlC_2 and $Mo_2Ti_2AlC_3$. *J. Appl. Phys.* **2015**, *118*, 94304.

(31) Anasori, B.; Xie, Y.; Beidaghi, M.; Lu, J.; Hosler, B. C.; Hultman, L.; Kent, P. R. C.; Gogotsi, Y.; Barsoum, M. W. Two-Dimensional, Ordered, Double Transition Metals Carbides (MXenes). *ACS Nano* **2015**, *9*, 9507–9516.

(32) Dahlqvist, M.; Rosén, J. Order and Disorder in Quaternary Atomic Laminates from First-Principles Calculations. *Phys. Chem. Chem. Phys. -PCCP J. Name* **2015**, *47*, 31810–31821.

(33) Hume-Rothery, W. The Structure of Metals and Alloys. *J. Chem. Educ.* **1936**, *13*, 350.

(34) Song, M. S.; Huang, B.; Zhang, M. X.; Li, J. G. In Situ Synthesis of ZrC Particles and

Its Formation Mechanism by Self-Propagating Reaction from Al-Zr-C Elemental Powders. *Powder Technol.* **2009**, *191*, 34–38.

(35) Wyckoff, R. W. G. Crystal Structures. *Intersci. Publ., New York* **1963**, 1.

(36) Adjaoud, O.; Steinle-Neumann, G.; Burton, B. P.; Van De Walle, A. First-Principles Phase Diagram Calculations for the HfC-TiC, ZrC-TiC, and HfC-ZrC Solid Solutions. *Phys. Rev. B - Condens. Matter Mater. Phys.* **2009**, *80*, 32–34.

(37) Razumovskiy, V. I.; Ruban, A. V; Odqvist, J.; Dilner, D.; Korzhavyi, P. A. Effect of Carbon Vacancies on Thermodynamic Properties of TiC – ZrC Mixed Carbides. *CALPHAD Comput. Coupling Phase Diagrams Thermochem.* **2014**, *46*, 87–91.

For Table of Contents Only

$(Zr,Ti)_2AlC$ and $(Zr,Ti)_3AlC_2$ MAX phases were experimentally synthesised. To our knowledge, this is the first report on the synthesis of $(Zr,Ti)_2AlC$ and the observation of ordering in $(Ti_{0.67},Zr_{0.33})_3AlC_2$ MAX phases. Experimental evidence of the ordering in $(Zr,Ti)_4AlC_3$ was also presented.